Journal of Alloys and Compounds 509 (2011) 6418–6422

Contents lists available at ScienceDirect

Journal of Alloys and Compounds

journal homepage: www.elsevier.com/locate/jallcom

Preparation and luminescence properties of lutetium oxide hollow spheres by a template-directed route

Guang Jia [a,*], Cuimiao Zhang [a], Liyong Wang [a], Shiwen Ding [a], Hongpeng You [b,*]

[a] College of Chemistry and Environmental Science, Hebei University, Baoding 071002, PR China
[b] State Key Laboratory of Rare Earth Resource Utilization, Changchun Institute of Applied Chemistry, Chinese Academy of Sciences, Changchun 130022, PR China

ARTICLE INFO

Article history:
Received 21 December 2010
Received in revised form 10 March 2011
Accepted 10 March 2011
Available online 21 March 2011

Keywords:
Lutetium oxide
Hollow spheres
Synthesis
Luminescence properties

ABSTRACT

Well-dispersed lutetium oxide (Lu_2O_3) hollow spheres have been obtained by a template-directed method with carbon spheres as template followed by a heat treatment. The main synthesis process was carried out in aqueous condition without any organic solvents, surfactant, or etching agents. SEM and TEM images reveal that the Lu_2O_3 hollow spheres inherit the spherical shape and good dispersion of carbon spheres, and the shells of the hollow spheres are composed of a large amount of uniform nanoparticles. The lanthanide activator ions doped Lu_2O_3 hollow spheres show intense down- and upconversion luminescence with different colors under ultraviolet or 980 nm light excitation, which may find potential applications in the fields of drug delivery or biological labeling. Furthermore, the luminescent mechanisms of the luminescent hollow spheres were investigated.

1. Introduction

In modern chemistry and materials science, the precisely architectural manipulation of nano/microcrystals with well-defined morphologies and tunable sizes remains the research focus, because the properties of the materials closely interrelate with geometrical factors such as shape, dimensionality, and size [1,2]. Among the various nano/microstructures, hollow nano/microspheres currently represent one of the fastest growing areas in comparison with other structural features [3,4]. The possibility of modifying the outer and inner surfaces may enhance the advantageous characteristics of hollow spheres. Owing to the distinct low effective density, high specific surface area, and encapsulation ability, the hollow spheres are considered to be promising materials in many fields such as catalysis [5], photonic devices [6], electrochemical cells [7], and biotechnology [8]. Recently, different methods for the design and fabrication of hollow spherical materials have been developed. Among them, template-directed synthesis with hard templates or soft templates has been proved to be an effective approach to fabricate inorganic hollow spheres [9–11]. To date, many inorganic hollow nano/microspheres have been successfully prepared via the template-directed synthesis route, such as C [12], TiO_2 [13], Co_3O_4 [14], YPO_4 [15], and $NaYF_4$ [16].

Much research attention has been paid to the synthesis of lanthanide compounds, because they can be used as high-performance phosphors, catalysts, and other functional materials due to their novel electronic, optical, and chemical properties [17–20]. Lutetium oxide (Lu_2O_3) is an excellent candidate due to its favorable physical properties, such as high melting point, phase stability, and low thermal expansion. Ln^{3+}-doped Lu_2O_3 (Ln = Eu, Tb, Er, Ho, Sm) materials have been proven to be important phosphors as reported in previous literatures [21–23]. Up to now, different morphologies of Lu_2O_3 have been prepared by various synthesis methods, such as nanorods [21], microflowers [22], nanocrystals [23], nanoflakes [24], and core–shell structures [25]. On the other hand, many lanthanide oxide hollow spheres have been synthesized via template-directed routes, such as Y_2O_3 [26,27], Gd_2O_3 [20], and CeO_2 [28]. However, to our knowledge, little attention has been paid to the synthesis of Ln^{3+}-doped luminescent Lu_2O_3 hollow spheres. Recently, we have successfully synthesized the micrometer-sized Lu_2O_3 hollow spheres with luminescent properties by using MF resin spheres as template [29]. The diameters of the Lu_2O_3 hollow microspheres are about 1.8 μm, which may limit their applications in biological fields.

In the present study, we have utilized homogeneous precipitation method to fabricate nanoscaled Lu_2O_3 hollow spheres with colloidal carbon spheres as template. The structure, morphology, formation process and luminescence properties (down- and upconversion emissions) of the hollow spheres were investigated in detail.

* Corresponding authors. Tel.: +86 431 5971111; fax: +86 431 5079505.
E-mail addresses: guangjia2001@yahoo.cn (G. Jia), hpyou@ciac.jl.cn (H. You).

0925-8388/$ – see front matter © 2011 Elsevier B.V. All rights reserved.
doi:10.1016/j.jallcom.2011.03.075

2. Experimental

2.1. Synthesis

$Ln(NO_3)_3$ (Ln = Lu, Eu, Yb, and Er) aqueous solutions were prepared by dissolving Ln_2O_3 (99.99%) in dilute HNO_3 solution under heating with agitation. All the other chemicals were of analytical grade reagents and were used directly without further purification.

The synthesis of carbon sphere template was carried out in a Teflon-lined stainless steel autoclave. The synthesis method has been described elsewhere previously in detail [27]. In a typical synthesis of Lu_2O_3 hollow spheres, 1 mmol of $Lu(NO_3)_3$ aqueous solution (2 mL) was added to 25 mL of deionized water. Then 3.0 g of urea was dissolved in the solution to form a clear solution by stirring. Subsequently, 0.15 g of carbon spheres was added and well dispersed into the above solution with the assistance of ultrasonication for 15 min. Then, the mixture was transferred into a round bottom flask and heated at 85 °C for 3 h with vigorous stirring. The precursor was collected by centrifugation and washed by deionized water and ethanol and dried at 60 °C in air. The final Lu_2O_3 hollow spheres were obtained through a calcination process at 800 °C for 2 h in air with a heating rate of 2 °C min^{-1}.

A similar process was employed to prepare Lu_2O_3:5%Eu^{3+}, Lu_2O_3:1%Er^{3+} and Lu_2O_3:5%Yb^{3+}, 1%Er^{3+} hollow spheres by using stoichiometric amount of $Eu(NO_3)_3$, $Er(NO_3)_3$, and/or $Yb(NO_3)_3$ aqueous solutions instead of $Lu(NO_3)_3$ solution for the precursors at initial stage as described above (total amount of Ln^{3+} was kept at 1 mmol).

2.2. Characterization

The powder X-ray diffraction (XRD) was performed on a D8 Focus diffractometer (Bruker). Thermogravimetric analysis and differential scanning calorimetry (TGA–DSC) data were recorded with a thermal analysis instrument (SDT 2960, TA Instruments, New Castle, DE). The morphology of the samples was inspected by a scanning electron microscope (SEM; S-4800, Hitachi). Transmission electron microscopy (TEM) images and selected area electron diffraction (SAED) patterns were obtained by an FEI Tecnai G2 S-Twin transmission electron microscope. The excitation and emission spectra were recorded with a Hitachi F-4500 spectrophotometer equipped with a xenon lamp as the excitation source. The luminescence decay curves were obtained from a Lecroy Wave Runner 6100 Digital Oscilloscope (1 GHz) using a tunable laser as the excitation (Continuum Sunlite OPO). The upconversion (UC) emission spectra were obtained using a 980 nm laser from an OPO as the excitation source and detected by R955 (Hamamatsu). All measurements were performed at room temperature.

3. Results and discussion

3.1. Phase identification and morphology

Fig. 1 shows the XRD patterns of the precursor, pure and Ln^{3+}-doped Lu_2O_3 after calcination at 800 °C. No obvious diffraction peak can be observed from the precursor (Fig. 1a), revealing that the precursor is amorphous. The component of the precursor is assigned to be $Lu(OH)CO_3$ according to the previous literatures [27,29–31]. After the annealing process, all the diffraction peaks of the pure and Ln^{3+} doped products can be indexed to the cubic phase of Lu_2O_3 [JCPDS No. 86-2475; space group: $Ia\bar{3}(206)$] (Fig. 1b–e), and no other impurity peaks can be detected. On the basis of the (2 2 2) crystal plane (d = 2.9985 Å), the lattice constant a of Lu_2O_3 sample is calculated to be 10.387 Å, which is well compatible with the standard value of a = 10.391 Å (JCPDS No. 86-2475). As the ionic radius of Lu^{3+} is smaller than those of doped activator ions, the diffraction peaks of the Lu_2O_3:Ln^{3+} (Ln = Er, Yb, or Eu) samples slightly shift to the lower angle side in comparison with that of the pure Lu_2O_3 sample, revealing that the activator ions have been effectively doped into the Lu_2O_3 host lattice. The very sharp and strong diffraction peaks mean high crystallinity, revealing less traps and stronger luminescence of the Lu_2O_3:Ln^{3+} samples, which is important for application as a luminescent material.

The thermal behaviors of the as-obtained precursor were investigated by TGA–DSC measurements. Fig. 2 shows TGA–DSC curves of the precursor. There is a major stage of sharp weight loss in the TG curve at 422 °C (Fig. 2a), accompanying the corresponding exothermic peak in the DSC curve (Fig. 2b). The rapid weight loss can be attributed to the dehydration and burning of the carbon spheres

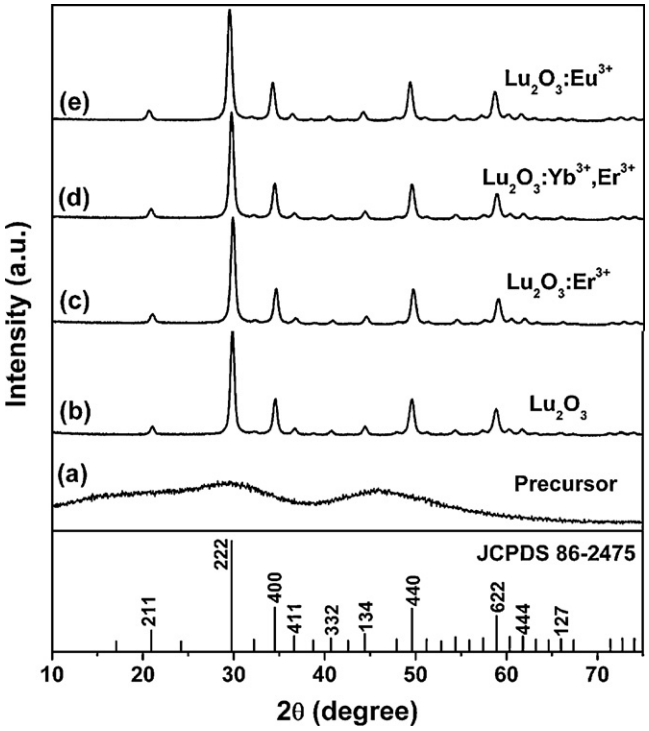

Fig. 1. XRD patterns of the samples for (a) uncalcined precursor, (b) Lu_2O_3, (c) Lu_2O_3:5%Eu^{3+}, (d) Lu_2O_3:1%Er^{3+}, and (e) Lu_2O_3:5%Yb^{3+}/1%Er^{3+} after calcination at 800 °C for 2 h. The standard data for cubic phase Lu_2O_3 (JCPDS No. 86-2475) is presented for comparison.

template. In addition, a slight weight loss accompanied with a broad weak endothermic peak can be observed from 550 to 750 °C, which can be assigned to the conversion from the amorphous precursor to the crystalline Lu_2O_3. The residual weight percentage of the precursor is about 43.3%, which accounts for the final Lu_2O_3 hollow spheres.

The SEM image of the carbon spheres shows that the template consists of well-dispersed nanospheres with diameters in the range of 300–400 nm (Fig. 3a), and the surfaces of carbon spheres are smooth. Fig. 3b shows the SEM image of the precursor before calcination. One can see that the precursor inherits the spherical morphology, and the surfaces of precursor particles are much rougher than those of carbon spheres due to the precipitation of

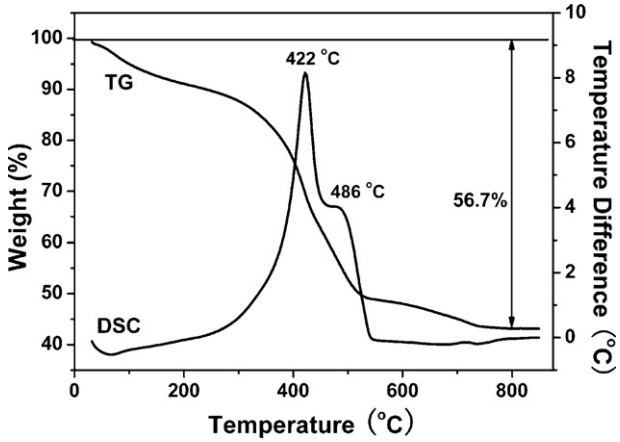

Fig. 2. TGA–DSC curves of the core–shell structured precursor.

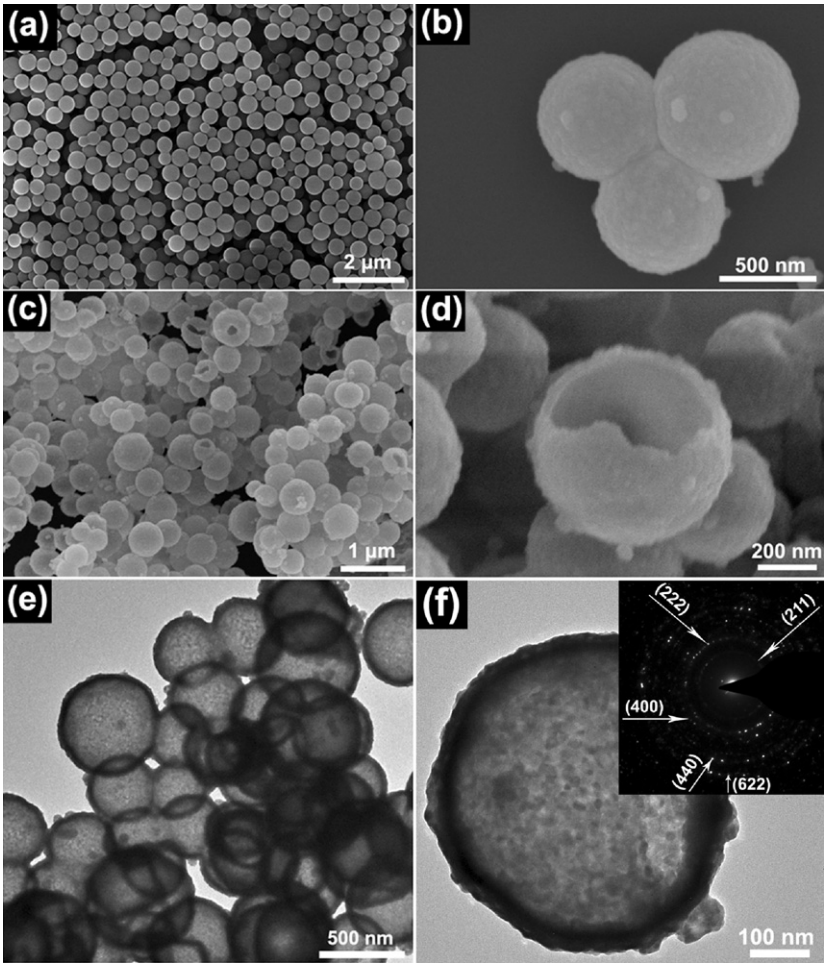

Fig. 3. SEM images of (a) carbon spheres, (b) precursor, and (c and d) Lu_2O_3 hollow spheres. (e and f) TEM images of Lu_2O_3 hollow spheres. Inset in (f) is the corresponding SAED pattern of a single hollow sphere.

a large amount of uniform nanoparticles. Naturally, the size of the precursor particles is a little larger than those of bare carbon spheres due to the Lu(OH)CO_3 shell. Fig. 3c–f shows the morphology of the Lu_2O_3 sample after calcination at 800 °C. Fig. 3c illuminates the panoramic SEM image of the Lu_2O_3 sample, which indicates that the sample consists of a large scale of well-dispersed hollow spheres. The result reveals that the carbon sphere template essentially determines the morphology of the Lu_2O_3 products. From the enlarged SEM image, one can observe a small quantity of ruptured hollow spheres (Fig. 3d), which can provide evidence that the spheres are of hollow structure. The rupture of the spheres may be caused by the releasing of gaseous carbon oxides when the oxidation process of carbon spheres occurred in the calcination process. Moreover, the wall thickness of hollow spheres is estimated to be about 40 nm from the ruptured hollow spheres. To provide further insight into the hollow spheres, TEM measurement was also performed. The TEM image of the Lu_2O_3 sample exhibits the spherical morphology with good dispersion (Fig. 3e), agreeing well with the SEM images. The strong contrast between the dark edge and the pale center reveals the hollow nature of the spheres. The wall thickness of the shell is about 40 nm from the enlarged TEM image (Fig. 3f), which is in accordance with the SEM result (Fig. 3d). The corresponding SAED pattern (inset in Fig. 3f) taken from a hollow sphere can be indexed as the (2 1 1), (2 2 2), (4 0 0), (4 4 0), and (6 2 2) reflections of the cubic Lu_2O_3, which agrees well with the XRD results [21,25].

3.2. Luminescent properties

It is well-known that the lutetium oxide (Lu_2O_3) is an excellent host lattice for down- and upconversion luminescence of various optically active rare earth ions due to its favorable physical properties. In the present study, a stoichiometric amount of lanthanide ions (Eu^{3+}, Er^{3+}, and Yb^{3+}) was doped into the Lu_2O_3 hollow spheres to investigate the luminescence properties. The crystalline Lu_2O_3 belongs the cubic system with space group *Ia*3 whose structure is similar to that of Y_2O_3. This type of structure contains two crystallographically different cation sites with *C2* and *S6* symmetry, respectively. The doped lanthanide ions are assumed to occupy these two types of sites in a statistical way [32,33].

The Lu_2O_3:5%Eu^{3+} hollow spheres exhibit strong red emission under ultraviolet (UV) excitation, which are similar to other Lu_2O_3:Eu^{3+} phosphors [21,24,25]. The excitation spectrum consists of a strong broadband at about 252 nm and some weak lines (324, 396, 469 nm) in the longer wavelength region, which are ascribed to the charge-transfer band (CTB) between the O^{2-} and Eu^{3+} and the f–f transition of the Eu^{3+} ions, respectively (Fig. 4a). Upon excitation at 252 nm, the emission spectrum is composed of a group of lines peaking at 579, 592 (586, 598), 610, 649, and 705 nm, which are assigned to the $^5D_0$–^7F_J (J = 0, 1, 2, 3, 4) transitions of the Eu^{3+} ions, respectively (Fig. 4b). The emission spectrum is dominated by the red $^5D_0$–$^7F_2$ (610 nm) transition of the Eu^{3+} ions. The hypersensitive transition $^5D_0$–$^7F_2$ (610 nm) is electronic dipole allowed.

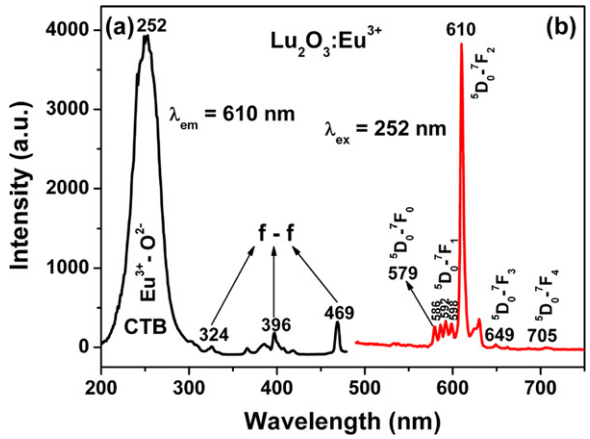

Fig. 4. Photoluminescence (a) excitation and (b) emission spectra of $Lu_2O_3:Eu^{3+}$ hollow spheres.

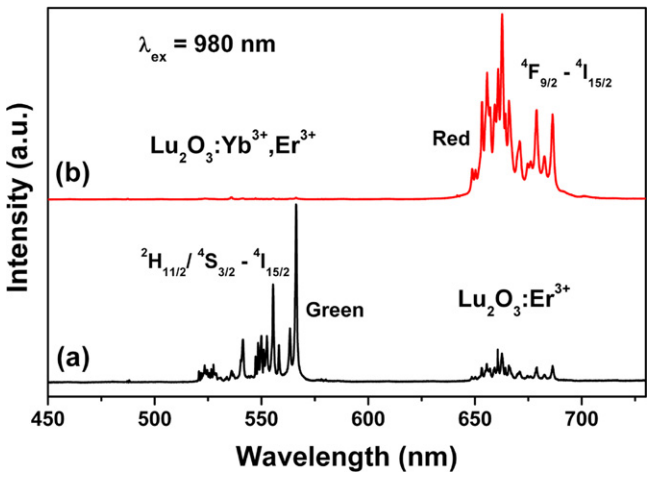

Fig. 6. Upconversion luminescence spectra of (a) $Lu_2O_3:Er^{3+}$ and (b) $Lu_2O_3:Yb^{3+},Er^{3+}$ hollow spheres under 980 nm light excitation.

So it depends on the local electric field and, hence, local symmetry. It is well-established that there are two Lu^{3+} sites in cubic Lu_2O_3; 75% of these sites are noncentrosymmetric with *C2* symmetry, and 25% are centrosymmetric, having *S6* symmetry [32,33]. When the Eu^{3+} ions are located at a low-symmetry local site without an inversion center, this forced-electric dipole transition is often dominant in the emission spectrum. So the strongest $^5D_0$–$^7F_2$ transition and nearly all of other features in the spectrum are due to the Eu^{3+} on *C2* site. The $^5D_0$–$^7F_0$ (579 nm) transition of Eu^{3+}, which is strongly forbidden for *S6* site, is also from Eu^{3+} (*C2* site). However, the three $^5D_0$–$^7F_1$ transition lines (586, 592, 598 nm) which are allowed for both *C2* and *S6* sites, are expected to arise from both *C2* and *S6* sites [34,35].

Fig. 5 shows the decay curve for the luminescence of the $^5D_0$–$^7F_2$ transition of the Eu^{3+} ions in Lu_2O_3 host lattice. The decay curve of $Lu_2O_3:Eu^{3+}$ hollow spheres can be fitted into a single-exponential function. The lifetime of the Eu^{3+} ions is determined to be 0.95 ms, which basically agrees with other $Lu_2O_3:Eu^{3+}$ phosphors reported in the previous literatures [21,22,36].

Fig. 6 shows the upconversion (UC) luminescence spectra of Lu_2O_3:1%Er^{3+} and Lu_2O_3:5%Yb^{3+}, 1%Er^{3+} samples under 980 nm light excitation, respectively. The UC emission spectrum of $Lu_2O_3:Er^{3+}$ sample is composed of a series of intense emission lines in the green region and a group of weak emission lines in the red region (Fig. 6a). The series of emission lines between 520 and 570 nm can be attributed to the $^2H_{11/2}$–$^4I_{15/2}$ and $^4S_{3/2}$–$^4I_{15/2}$ transitions of the Er^{3+} ions, and the emission lines centered at about 662 nm are assigned to the $^4F_{9/2}$–$^4I_{15/2}$ transition of Er^{3+} ions, respectively. As we know, the codoping does not only increase the efficiency of luminescence, but also induces UC luminescence between the donor and acceptor ions [23,37,38]. Here, Yb^{3+} was chosen as the co-dopant with Er^{3+}, because it possesses a large absorption cross section at 980 nm, and the energy transfer occurs as a result of the spectral overlap between the Yb^{3+} $^2F_{5/2}$–$^2F_{7/2}$ emission and the Er^{3+} $^4I_{11/2}$–$^4I_{15/2}$ absorption bands. The UC luminescence spectrum of $Lu_2O_3:Yb^{3+},Er^{3+}$ hollow spheres mainly includes strong red emission corresponding to the $^4F_{9/2}$–$^4I_{15/2}$ transition of the Er^{3+} ions, together with the weak green emissions assigned to the $^2H_{11/2}$–$^4I_{15/2}$ and $^4S_{3/2}$–$^4I_{15/2}$ transitions of the Er^{3+} ions, respectively (Fig. 6b).

To better understand the UC mechanism of Yb^{3+} and Er^{3+} ions in Lu_2O_3 matrix, the UC emission intensity (I) was measured as a function of the laser power (P) (Fig. 7). For the upconversion process, I is proportional to the nth power of P, that is:

$$I \propto P^n$$

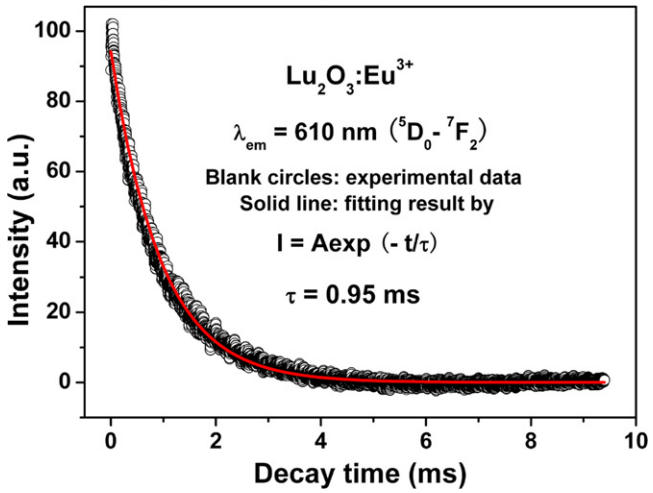

Fig. 5. Decay curve for the $^5D_0$–$^7F_2$ (610 nm) emission of Eu^{3+} in $Lu_2O_3:Eu^{3+}$ hollow spheres.

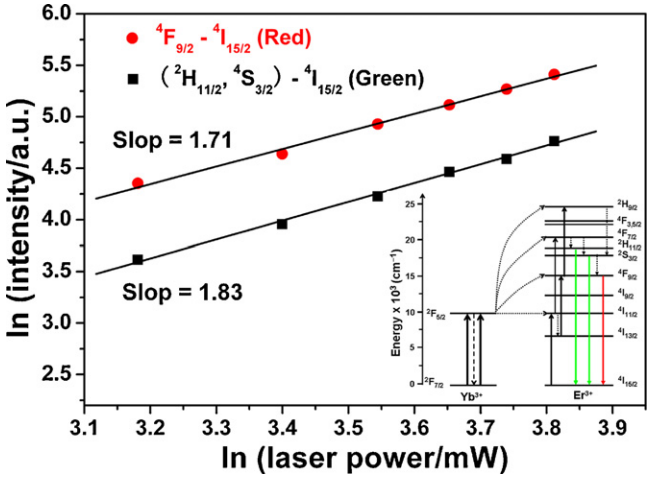

Fig. 7. Power dependence of UC emission intensities of ($^2H_{11/2}$, $^4S_{3/2}$)–$^4I_{15/2}$ transition in $Lu_2O_3:Er^{3+}$ and $^4F_{9/2}$–$^4I_{15/2}$ transition in $Lu_2O_3:Yb^{3+},Er^{3+}$ under 980 nm excitation. Inset: Energy-level diagram of Yb^{3+},Er^{3+}-codoped sample and UC emission processes.

where n is the number of pump photons absorbed per upconverted photon emitted [39–41]. A plot of $\ln I$ versus $\ln P$ yields a straight line with slope n. Fig. 7 shows the results for the ($^2H_{11/2}$, $^4S_{3/2}$)–$^4I_{15/2}$ green emission and $^4F_{9/2}$–$^4I_{15/2}$ red emission of the Er^{3+} ions. The calculated results indicate that slopes n are 1.71 and 1.83 for red and green emissions, respectively. The result indicates that the UC mechanism corresponding to both green and red emissions occurs via a two-photon process. As indicated in the energy level diagram of Yb^{3+} and Er^{3+} ions (inset in Fig. 7), an initial energy transfer from an Yb^{3+} ion in the $^2F_{5/2}$ state to an Er^{3+} ion populates the $^4I_{11/2}$ level of Er^{3+}. Subsequent nonradiative relaxations of $^4I_{11/2}$–$^4I_{13/2}$ also populate the $^4I_{13/2}$ level. Then, a second 980 nm photon transferred by the excited Yb^{3+} ions can then populate a higher $^4F_{7/2}$ state from $^4I_{11/2}$ of the Er^{3+} ions (or populate $^4F_{9/2}$ state from $^4I_{13/2}$) through energy transfer. Then, the Er^{3+} ions relax nonradiatively by a fast multiphoton decay process to the $^2H_{11/2}$ and $^4S_{3/2}$ levels and the dominant ($^2H_{11/2}$, $^4S_{3/2}$)–$^4I_{15/2}$ green emissions occur. Alternatively, the electron can further relax and populate the $^4F_{9/2}$ level. The populated $^4F_{9/2}$ level of the Er^{3+} ion relaxes to the $^4I_{15/2}$ ground-state level, resulting in the red emission [39].

The UC emission spectra shows that the emission color changes evidently from green to red when Yb^{3+} ion was codoped with Er^{3+} into Lu_2O_3 host lattice, which agrees well with the previous literatures [37–39,42]. This case is caused by fewer Er^{3+} ions holding at the green-emitting levels ($^2H_{11/2}$/$^4S_{3/2}$) and more Er^{3+} ions holding at the red-emitting level ($^4F_{9/2}$). An elevated amount of Yb^{3+} ions in the Lu_2O_3 host lattice would decrease Yb–Er interatomic distance and thus facilitate back-energy-transfer from Yb^{3+} to Er^{3+} (inset in Fig. 7). Then, the energy transfer suppresses the population in excited levels of $^2H_{11/2}$ and $^4S_{3/2}$, resulting in the decrease of green emissions. Meanwhile, the energy transfer leads to the saturation of the $^4I_{13/2}$ state of Er^{3+} and the excited Yb^{3+} ions transfer its energy to Er^{3+} ions via the energy-transfer process [$^2F_{5/2}$ (Yb^{3+}) + $^4I_{13/2}$ (Er^{3+}) → $^2F_{7/2}$ (Yb^{3+}) + $^4F_{9/2}$ (Er^{3+})], which can directly populate the $^4F_{9/2}$ level, resulting in the enhancement of red emission [23,43].

4. Conclusions

The well-dispersed Lu_2O_3 hollow spheres have been successfully fabricated via a template-directed method. The precursors were first synthesized by a homogeneous precipitation technique with carbon spheres as template. Subsequently, the template was removed and the Lu_2O_3 hollow spheres were obtained during a calcination process. The as-obtained Lu_2O_3:Eu^{3+} hollow spheres exhibit red emission under UV excitation, and the Lu_2O_3:Er^{3+} and Lu_2O_3:Yb^{3+},Er^{3+} samples show green and red emissions under 980 nm light excitation, respectively. The experimental result and analysis reveal that the two-photon process should be responsible for the upconversion luminescence of Yb^{3+} and Er^{3+} doped samples. Moreover, the as-synthesized Lu_2O_3:Ln^{3+} hollow spheres may find potential applications in biological fields.

Acknowledgments

This work is financially supported by the Research Plan of the National Natural Science Foundation of Hebei University, the Fund for Creative Research Groups (Grant No. 20921002), and the National Basic Research Program of China (973 Program, Grant No. 2007CB935502).

References

[1] J. Hu, T.W. Odom, C.M. Lieber, Acc. Chem. Res. 32 (1999) 435–445.
[2] F. Lei, B. Yan, H.H. Chen, Q. Zhang, J.T. Zhao, Cryst. Growth Des. 9 (2009) 3730–3736.
[3] H.S. Im, U. Jeong, Y. Xia, Nat. Mater. 4 (2005) 671–675.
[4] X. Feng, L. Yang, N. Zhang, Y. Liu, J. Alloys Compd. 506 (2010) 728–733.
[5] X. Xie, H. Yang, F. Zhang, L. Li, J. Ma, H. Jiao, J. Zhang, J. Alloys Compd. 477 (2009) 90–99.
[6] X.L. Xu, S.A. Asher, J. Am. Chem. Soc. 126 (2004) 7940–7945.
[7] Y. Li, W. Li, S. Chou, J. Chen, J. Alloys Compd. 456 (2008) 339–343.
[8] A.N. Zelikin, Q. Li, F. Caruso, Angew. Chem. Int. Ed. 45 (2006) 7743–7745.
[9] Y. Zeng, X. Wang, H. Wang, Y. Dong, Y. Ma, J.N. Yao, Chem. Commun. 46 (2010) 4312–4314.
[10] Y.Q. Wang, G.Z. Wang, H.Q. Wang, C.H. Liang, W.P. Cai, L.D. Zhang, Chem. Eur. J. 16 (2010) 3497–3503.
[11] J. Zheng, B.H. Wu, Z.Y. Jiang, Q. Kuang, X.L. Fang, Z.X. Xie, R.B. Huang, L.S. Zheng, Chem. Asian J. 5 (2010) 1439–1444.
[12] L.M. Guo, L.X. Zhang, J.L. Shi, Mater. Lett. 65 (2011) 1–3.
[13] C. Wang, Y.H. Ao, P.F. Wang, J. Hou, J. Qian, Appl. Surf. Sci. 257 (2010) 227–231.
[14] L. Yang, W. Guan, B. Bai, Q. Xu, Y. Xiang, J. Alloys Compd. 504 (2010) L10–L13.
[15] L. Zhang, G. Jia, H. You, K. Liu, M. Yang, Y. Song, Y. Zheng, Y. Huang, N. Guo, H. Zhang, Inorg. Chem. 49 (2010) 3305–3309.
[16] F. Zhang, Y. Shi, X. Sun, D. Zhao, G.D. Stucky, Chem. Mater. 21 (2009) 5237–5243.
[17] T. Suehiro, N. Hirosaki, R.J. Xie, T. Sato, Appl. Phys. Lett. 95 (2009) 051903.
[18] Q. Mu, Y. Wang, J. Alloys Compd. 509 (2011) 396–401.
[19] G. Jia, H. You, K. Liu, Y. Zheng, N. Guo, J. Jia, H. Zhang, Chem. Eur. J. 16 (2010) 2930–2937.
[20] Y. Liu, P. Yang, W. Wang, H. Dong, J. Lin, CrystEngComm 12 (2010) 3717–3723.
[21] G. Jia, Y. Zheng, K. Liu, Y. Song, H. You, H. Zhang, J. Phys. Chem. C 113 (2009) 153–158.
[22] J. Yang, C.X. Li, Z.W. Quan, C.M. Zhang, P.P. Yang, Y.Y. Li, C.C. Yu, J. Lin, J. Phys. Chem. C 112 (2008) 12777–12785.
[23] J. Yang, C.M. Zhang, C. Peng, C.X. Li, L.L. Wang, R.T. Chai, J. Lin, Chem. Eur. J. 15 (2009) 4649–4655.
[24] J. Wang, Q. Liu, Q.F. Liu, J. Mater. Chem. 15 (2005) 4141–4146.
[25] Y.V. Yermolayeva, A.V. Tolmachev, T.I. Korshikova, R.P. Yavetskiy, M.V. Dobrotvorskaya, N.I. Danylenko, D.S. Sofronov, Nanotechnology 20 (2009) 325601.
[26] G. Jia, H. You, Y. Song, Y. Huang, M. Yang, H. Zhang, Inorg. Chem. 49 (2010) 7721–7725.
[27] G. Jia, M. Yang, Y. Song, H. You, H. Zhang, Cryst. Growth Des. 9 (2009) 301–307.
[28] X.Z. Li, F. Chen, X.W. Lu, C.Y. Ni, X.B. Zhao, Z.G. Chen, J. Porous Mater. 17 (2010) 297–303.
[29] G. Jia, H. You, Y. Zheng, K. Liu, N. Guo, H. Zhang, CrystEngComm 12 (2010) 2943–2948.
[30] J.G. Li, X.D. Li, X.D. Sun, T. Ikegami, T. Ishigaki, Chem. Mater. 20 (2008) 2274–2281.
[31] J.G. Li, X.D. Li, X.D. Sun, T. Ishigaki, J. Phys. Chem. C 112 (2008) 11707–11716.
[32] E. Zych, M. Karbowiak, K. Domagala, S. Hubert, J. Alloys Compd. 341 (2002) 381–384.
[33] J.C. Park, H.K. Moon, D.K. Kim, S.H. Byeon, B.C. Kim, K.S. Suh, Appl. Phys. Lett. 77 (2000) 2162–2164.
[34] K. Binnemans, C. Gorller-Walrand, J. Rare Earth 14 (1996) 173–180.
[35] M.L. Pang, J. Lin, J. Fu, R.B. Xing, C.X. Luo, Y.C. Han, Opt. Mater. 23 (2003) 547–558.
[36] J.C. Wang, Q. Liu, Q.F. Liu, Opt. Mater. 29 (2007) 593–597.
[37] G.K. Das, T.Y. Tan, J. Phys. Chem. C 112 (2008) 11211–11217.
[38] D. Matsuura, Appl. Phys. Lett. 81 (2002) 4526–4528.
[39] X. Bai, H. Song, G. Pan, Y. Lei, T. Wang, X. Ren, S. Lu, B. Dong, Q. Dai, L. Fan, J. Phys. Chem. C 111 (2007) 13611–13617.
[40] H. Guo, N. Dong, M. Yin, W. Zhang, L. Lou, S. Xia, J. Phys. Chem. B 108 (2004) 19205–19209.
[41] Y. Sun, H. Liu, X. Wang, X. Kong, H. Zhang, Chem. Mater. 18 (2006) 2726–2732.
[42] Y.P. Li, J.H. Zhang, X. Zhang, Y.S. Luo, X.G. Ren, H.F. Zhao, X.J. Wang, L.D. Sun, C.H. Yan, J. Phys. Chem. C 113 (2009) 4413–4418.
[43] F. Wang, X.G. Liu, J. Am. Chem. Soc. 130 (2008) 5642–5643.